Inorganic Chemistry

Article

pubs.acs.org/IC

Synthesis, Characterization, Photocatalysis, and Varied Properties of TiO_2 Cosubstituted with Nitrogen and Fluorine

Nitesh Kumar, Urmimala Maitra, Vinay I. Hegde, Umesh V. Waghmare, A. Sundaresan, and C. N. R. Rao*

Chemistry and Physics of Materials Unit, New Chemistry Unit, Theoretical Sciences Unit, and International Centre for Materials Science, Jawaharlal Nehru Centre for Advanced Scientific Research, Jakkur P.O., Bangalore-560064, India

ABSTRACT: TiO_2 (anatase) codoped with nitrogen and fluorine, synthesized by a simple solid state route, using urea and ammonium fluoride as sources of nitrogen and fluorine, respectively, as well as by decomposition of $(NH_4)_2TiF_6$ for comparison, has been characterized by various techniques. XPS analysis shows the composition to be $TiO_{1.7}N_{0.18}F_{0.12}$ for urea-based method (N, F-TiO_2-urea) and $TiO_{1.9}N_{0.04}F_{0.06}$ for complex decomposition method (N, F-TiO_2-complex). Both the materials are defect-free as revealed by photoluminescence spectroscopy. Thus, N, F-TiO_2-urea exhibits smaller defect-induced magnetization compared to the nitrogen-doped sample. Cosubstitution of N and F is accompanied with an enhancement of the absorption of light in the visible region giving rise to yellow color and with a band gap of ~2.2 eV in the case of N, F-TiO_2-urea. It exhibits enhanced photocatalytic activity and also significant hydrogen evolution (400 μmol/g) on interaction with visible light in the absence of any cocatalyst, which is much higher compared to N, F-TiO_2-complex and N-TiO_2. First-principles calculations show significant local distortions on codoping TiO_2 with N and F and a lowering of energy by 1.93 eV per N, F pair. With virtual negative and positive charges on nitrogen and fluorine, respectively, the dopants prefer pairwise clustering. Our calculations predict a reduction in the band gap in TiO_2 cosubstituted with nitrogen and fluorine. The calculated band structure shows that nitrogen 2p states form a separate subband just above the valence band which is enhanced on incorporation of fluorine. Our calculations also indicate anomalous Born effective charges in N, F-TiO_2 and predict enhanced photocatalytic activity on codoping of TiO_2 by N and F.

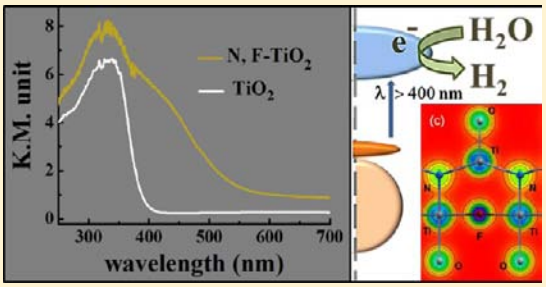

INTRODUCTION

Increasing energy demands and rapid consumption of fossil fuels have motivated a great deal of research on materials capable of producing hydrogen by reduction of water. Among them, TiO_2 has been an important material because of its band structure, high chemical and photostabilities, abundance and nontoxicity. A limitation, however, is that the visible region of the solar spectrum cannot be used with TiO_2. A considerable amount of work has been carried out in order to extend the absorption of TiO_2 to the visible region. Doping less electronegative atoms like N creates a band above the valence band of TiO_2 thereby narrowing the band gap.[1] Photocatalytic activity of N-TiO_2 has been studied by some workers.[2−4] Thus, Hashimoto and co-workers[4] have studied the decomposition of gaseous 2-propanol by N-TiO_2 with visible light. A disadvantage of nitrogen doping is that it creates oxygen vacancies which increase the electron−hole recombination rate. In contrast to the N-doping, fluorine doping in TiO_2 does not change the band gap because the p orbitals of fluorine are lower in energy than those of the less electronegative oxygen atoms. However, the strong electron-withdrawing ability of ≡Ti−F groups present on the surface of fluorine-doped TiO_2 makes the recombination of photogenerated electrons and holes difficult, allowing this material to be used as a better photocatalyst in the ultraviolet region than undoped TiO_2.[5−7] In order to achieve photocatalytic activity in the visible region, yet maintain the defect-free crystal structure, codoping of TiO_2 by nitrogen and a transition metal[8,9] as well as with nitrogen and fluorine has been attempted.[10−15] It is to be noted that one N atom and one F atom are equivalent to two oxygen atoms, and such cosubstitution would not create oxygen vacancies and other defects. Wang et al.[11] examined the synergistic effect of N and F codoping on the electronic structure of TiO_2 and its photocatalytic activity, while Liu et al.[14] studied water splitting by N, F-codoped TiO_2 prepared hydrothermally by relatively small starting from bulk TiN. The contents of N and F in the studies reported in the literature are relatively small. We considered it important to synthesize TiO_2 (anatase) with fairly high contents of N and F and study its properties. Toward this end, we have used urea instead of ammonia, ammonium halides, or melamine as the nitrogen source.[4,16−19] Urea is known to be an effective and cheap source of nitrogen for the synthesis of nitrides, oxynitrides, and N-doped oxides.[20−23] Starting with TiO_2 nanoparticles and using urea as the nitrogen source and NH_4F as the fluorine source, we have obtained N, F-codoped TiO_2 with relatively high percentages of both the dopants. We have investigated the optical, magnetic, and photocatalytic properties of N, F-TiO_2 in some detail. In order

Received: June 5, 2013
Published: September 5, 2013

   dx.doi.org/10.1021/ic401426q | *Inorg. Chem.* 2013, 52, 10512−10519

to understand the electronic structure and properties of N, F-TiO_2, we have carried out detailed first-principles calculations.

EXPERIMENTAL SECTION

TiO_2 nanoparticles were prepared by sol–gel method. In a typical synthesis,[24] 2 g of Pluronic P 123 was dissolved in 50 mL of 1 M NaCl aqueous solution. To this solution, 10 mL of titanium isopropoxide was added slowly and stirred at room temperature for 10 h. The white precipitate was centrifuged and washed several times with distilled water and ethanol. The product was dried at 80 °C for 10 h. The obtained powder was then heated in oxygen at 400 °C for 2 h. The TiO_2 powder so obtained was ground with excess of urea and NH_4F (10 times each by weight). The mixture was heated in nitrogen at 500 °C for 2 h to obtain yellow N, F-codoped TiO_2 powder (N, F-TiO_2-urea). For comparison, the starting TiO_2 was heated under similar conditions. N-doped TiO_2 was prepared by heating the starting TiO_2 powder at 800 °C for 5 h in ammonia. The product was heated in air at 450 °C for 30 min to obtain light yellow N-doped TiO_2 powder. N, F-codoped TiO_2 (N, F-TiO_2-complex) was also prepared by decomposing $(NH_4)_2TiF_6$ in air at 550 °C for 1 h according to a reported procedure.[25]

X-ray diffraction patterns were recorded in Bruker D8 Discover diffractometer and Rigaku-99 diffractometer using Cu Kα radiation. In order to obtain cell parameters of doped and undoped TiO_2 powders, Lebail fitting was carried out using *Fullprof* software.[26] X-ray photoelectron (XP) spectra were recorded in an Omicron Nanotechnology Spectrometer with Mg Kα as the X-ray source. Transmission electron microscopy studies were carried out in JEOL JEM 3010, fitted with a Gatan CCD camera operating at an accelerating voltage of 300 kV. UV–visible spectra were recorded in a Perkin-Elmer Lambda 900 UV/vis/NIR spectrometer in the diffuse reflectance mode. Photoluminescence spectra were recorded in Fluorolog-3 spectrophotometer from Horiba Jobin Yvon. Magnetic measurements were carried out in SQUID VSM (Quantum Design, U.S.).

In the dye degradation studies, 4 mg of catalyst was added to 10 mL of 30 μM methyl orange (MO) aqueous solution in a cylindrical quartz vessel, and the mixture was sonicated for 15 min followed by stirring for 30 min in the dark. The vessel was irradiated with the visible light by exposing it to a 400 W Xe lamp (Newport) fitted with 12 cm path length of water filter for removal of IR radiation along with a 400 nm cutoff filter. One milliliter of the mixture was taken out at an interval of 20 min for 2 h for recording UV–vis spectra in order to get the concentration of MO. Before taking the UV–vis spectra, the catalyst dispersed in the mixture was centrifuged out to avoid scattering.

Photocatalytic H_2 evolution experiments were carried out in a stoppered quartz vessel. A 400 W Xe lamp (Newport) fitted with 12 cm path length of water filter for removal of IR radiation and a 400 nm cutoff filter to block the UV light was used to irradiate the vessel. Photoreduction of H_2O into H_2 was carried out in aqueous solution containing 0.1 M Na_2SO_4 and 0.1 M Na_2S. Two milligrams of the catalyst was dispersed in 50 mL of water by ultrasonication, and the vessel was later purged with N_2 to remove all the gases before irradiation. The evolved gases were analyzed by gas chromatography using a Perkin-Elmer Clarus 580 GC. One millilter of the evolved gases was injected manually every 1 h for analysis.

COMPUTATIONAL DETAILS

Our first-principles calculations are based on density functional theory as implemented in Quantum ESPRESSO[27] and SIESTA[28] packages. In the ESPRESSO-based calculations, ultrasoft pseudopotentials[29] were used to model the interaction of ionic cores with electrons, and the exchange-correlation energy functional was approximated with a local density approximation (LDA) of the Perdew–Zunger form.[30] Kinetic energy cutoffs of 50 and 400 Ry were used for the representation of wave functions and charge density, respectively. Phonons and Born effective charges were calculated as second derivatives of energy within density functional perturbation theory (DFPT). Since the electronic band gap is underestimated in DFT-LDA calculations, we used hybrid density functionals based on a screened Coulomb potential for Hartree–Fock exchange (HSE),[31] to obtain more accurate estimates of the band gap and quantitatively confirm the experimental observations. Since ESPRESSO-based calculations were computationally expensive, we used SIESTA in our analysis of water adsorption on the (001) and (101) surfaces of nitrogen and fluorine-cosubstituted TiO_2. In the SIESTA-based calculations, we use Troullier–Martins[32] pseudopotentials to model ion–electron interactions and approximate the exchange-correlation energy functional with a Ceperly–Alder form[33] of LDA. We use atomic orbitals of the multiple-zeta kind with a split valence scheme as the basis with a split norm of 0.15 and the orbital-confining cutoff radii defined by an energy shift of 0.007 Ry.

RESULTS AND DISCUSSION

Experimental Results. Figure 1 shows the XRD patterns of undoped and N, F-TiO_2-urea, both of which crystallize in the

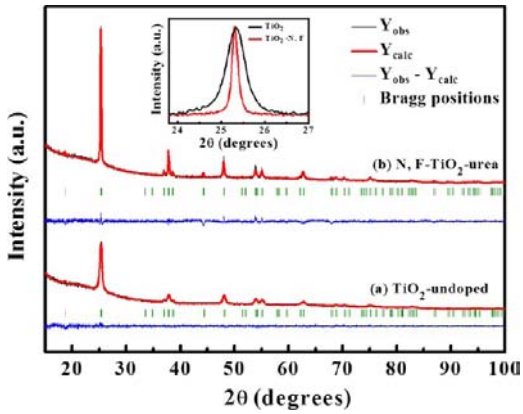

Figure 1. XRD patterns of (a) undoped TiO_2 and (b) N, F-TiO_2-urea. Inset shows magnified view of the (101) reflections.

anatase structure with the tetragonal space group $P4_2/mnm$, without any trace of the rutile phase. The cell parameters obtained by fitting the XRD patterns for the undoped TiO_2 and N, F-TiO_2-urea are a = 3.783(1) Å, c = 9.509(3) Å and a = 3.788(1) Å, c = 9.513 Å, respectively. The XRD pattern of N, F-TiO_2-urea exhibits sharper reflections (see inset of Figure 1 showing the (101) reflections). The crystallite sizes from the Scherrer formula are 16 and 51 nm for undoped and N, F-TiO_2-urea samples respectively.

Figure 2 shows the core-level X-ray photoelectron spectra (XPS) in the N 1s and F 1s regions of N, F-TiO_2-urea. Nitrogen-doped TiO_2 has been well characterized by XPS in terms of nature of N atoms at the surface and inside the crystal. The N 1s spectrum in Figure 2a can be deconvoluted into three peaks centered around 396.9, 398.4, and 401.0 eV. The signal at the lowest binding energy is ascribed to the nitrogen atom

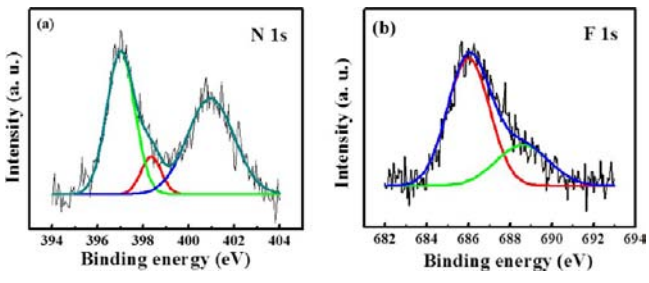

Figure 2. Core-level XP spectra in the (a) N 1s and (b) F 1s regions of N, F-TiO_2-urea.

dx.doi.org/10.1021/ic401426q | *Inorg. Chem.* 2013, 52, 10512–10519

directly bonded to Ti[34] and the signal around 398.4 eV to interstitial nitrogen atoms.[35] Surface-adsorbed nitrogen mostly present as NH gives rise to a peak at 401 eV.[10] The core-level spectrum of fluorine in Figure 2b can be deconvoluted into peaks centered around 686.0 and 688.6 eV. The more intense peak at 686.0 eV has been attributed to the formation of species such as $TiOF_2$ at the surface of the particles.[10] The peak at the higher binding energy (688.6 eV) is due to the substitution of fluorine in the oxygen site of TiO_2.[10,12,35] Taking the capture cross sections into account, the composition of the cosubstituted compound by taking only the signals at 396.9 and 688.6 eV for nitrogen and fluorine respectively works out to be $TiO_{1.7}N_{0.18}F_{0.12}$. If we take both 396.9 and 398.4 eV signals of N 1s and both the 686 and 688.6 eV signals of F 1s into consideration, the composition turns out to be $TiO_{1.47}N_{0.28}F_{0.25}$. Decomposing $(NH_4)_2TiF_6$ in air results in a moderate amount of nitrogen and fluorine codoping with a composition $TiO_{1.9}N_{0.04}F_{0.06}$. The TiO_2 sample doped only with nitrogen has the composition $TiO_{0.97}N_{0.03}$ as determined by XPS.

Figure 3 shows TEM images of undoped and N, F-TiO_2-urea samples. The average size of the undoped TiO_2 is found to be

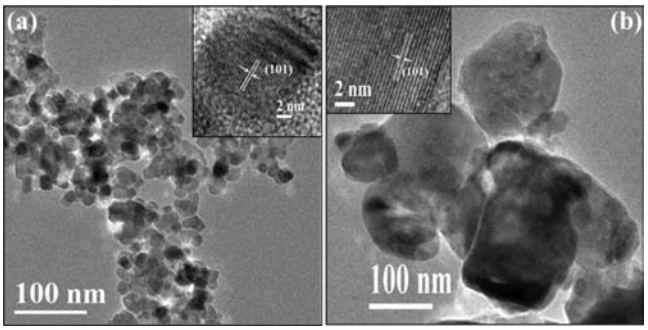

Figure 3. TEM images of (a) undoped TiO_2 and (b) N, F-TiO_2-urea. Inset shows the HREM images.

~15 nm as shown in Figure 3a. On cosubstitution of nitrogen and fluorine, the crystallite size grows considerably as shown in Figure 3b. These observations are consistent with the XRD results. Insets of Figures 3a and b show HREM images revealing the (101) lattice fringes, indicating the single crystalline nature of the particles.

In Figure 4a, we show the UV−visible spectra of undoped, N-doped, N, F-TiO_2-urea, and N, F-TiO_2-complex. The band edge in the undoped TiO_2 is observed at 393 nm (3.15 eV), consistent with the indirect band gap of anatase. Substitution with nitrogen causes only a small change in the spectrum with a weak broad feature around 450 nm. On cosubstituting with both nitrogen and fluorine by urea and ammonium fluoride, the white powder turns dark yellow (see Figure 4a). The absorption extends to the visible region with the band edge at 563 nm (2.2 eV). The band edge in the case of N, F-TiO_2-complex is found to be 496 nm (2.5 eV). The inset of Figure 4a shows Tauc's plot for all the four samples. Band-gap estimations are carried out using this plot. The absorption in the visible region in N, F-TiO_2-urea is significantly higher compared to the earlier reports of TiO_2.[4,11,36] This can be attributed to the high content of N and F in the sample prepared by us. It should be noted that when TiO_2 is heated in the urea alone, there is almost no substitution of nitrogen causing no change in the color and the band edge position. The presence of F appears to help in increasing the extent of N doping. We have also shown the UV−visible spectrum of F-TiO_2 which shows no detectable change in the band edge position compared to undoped TiO_2. Raman spectra of the codoped samples showed stiffening of the band corresponding to the symmetric stretching of the O−Ti−O bond.

Photoluminescence (PL) spectroscopy is a useful technique to study defects in oxides. PL spectra at an excitation wavelength of 400 nm of undoped, N-TiO_2, N, F-TiO_2-urea, and N, F-TiO_2-complex are shown in Figure 4b. A broad emission band centered around 600 nm can be clearly seen in N-TiO_2. The presence of this band is attributed to the oxygen vacancies.[37,38] The absence of defect band in codoped TiO_2 is expected because codoping of nitrogen and fluorine in the oxygen site maintains the charge balance in the oxide.

It has been established recently that room temperature ferromagnetism is a universal feature of otherwise nonmagnetic inorganic nanoparticles.[39,40] The origin of the ferromagnetism is attributed to the presence of defects such as cation or anion vacancies in the nanoparticles. Figure 5 shows the room temperature magnetization data of undoped and doped TiO_2 samples. We observe room temperature hysteresis in both the undoped and doped TiO_2 nanoparticles, but the saturation magnetization (M_S) of N-doped TiO_2 is highest with a value of 3.7×10^{-3} emu/g. This observation is consistent with the PL results, which show a broad oxygen defect related band in the case of N-doped TiO_2. For undoped and N, F-TiO_2-urea, where we do not observe any PL defect band, the values of M_S are 0.6×10^{-3} and 1.2×10^{-3} emu/g, respectively. These values are smaller than the value exhibited by N-doped TiO_2 (3.7×10^{-3} emu/g).

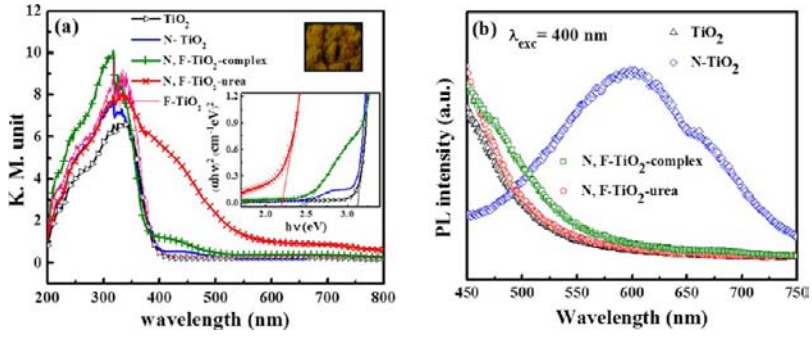

Figure 4. (a) UV−visible and (b) PL spectra of undoped TiO_2, N-doped, N, F-TiO_2-complex, and N, F-TiO_2-urea. Insets in (a) show the color of N, F-TiO_2-urea and the Tauc plot for all doped and undoped samples.

dx.doi.org/10.1021/ic401426q | Inorg. Chem. 2013, 52, 10512−10519

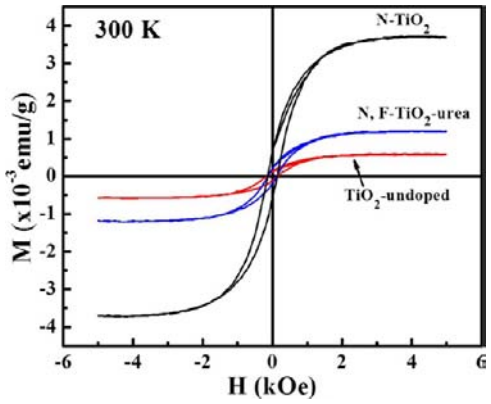

Figure 5. Magnetic hysteresis of undoped TiO_2, N-doped TiO_2, and N, F-TiO_2-urea at room temperature.

Dye degradation capability is employed as a measure of the photocatalytic activity of a material. We have studied the degradation of methyl orange (MO) to establish the photocatalytic activity of undoped TiO_2 and N, F-TiO_2-urea. MO is photostable in the absence of the catalyst unlike methylene blue which shows appreciable degradation in light without any catalyst. When exposed to light with wavelength >400 nm, MO degrades with a much faster rate in the presence of N, F-TiO_2-urea as compared to the undoped TiO_2 as shown in Figure 6.

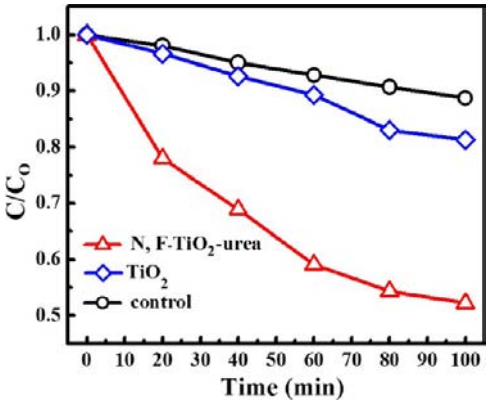

Figure 6. Degradation of methyl orange by undoped TiO_2 and N, F-TiO_2-urea on visible light irradiation (>400 nm) along with control.

Visible light MO degradation activity in N, F-TiO_2-urea is attributed to the high visible light absorption in the material. The mechanism of degradation of MO in the presence of TiO_2 is mainly due to the hole oxidation process at higher concentration of MO, while at the lower concentrations of MO, hydroxyl radicals (OH·) are more effective.[41] Results of control experiments with the dye irradiated under visible light (without any catalyst) are also included in Figure 6.

TiO_2 has been used to produce hydrogen by reducing water, since the minimum of the conduction band is more negative than water reduction potential. TiO_2 has, however, the disadvantage of having a high band gap which limits its use in the visible range of the solar spectrum. Nitrogen doping alone is capable of pushing the valence band toward higher energy to narrow the band gap, but codoping with nitrogen and fluorine maintains the charge balance in the system, resulting in eliminating defects or lowering the defect concentration and a substantial decrease in the band gap. Figure 7 shows the

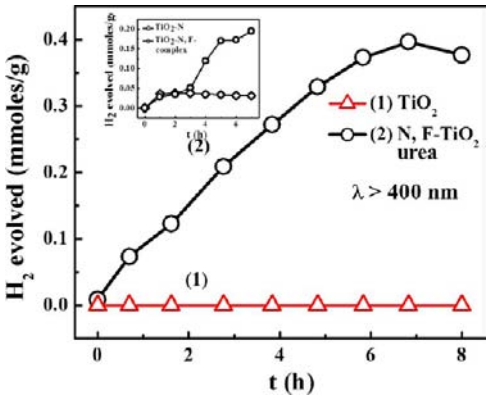

Figure 7. Hydrogen evolution with respect to time on irradiation with visible light (>400 nm) for undoped TiO_2 and N, F-TiO_2-urea. Inset shows the data for N-doped TiO_2 and N, F-TiO_2-complex.

evolution of hydrogen with time for undoped TiO_2 as well as N, F-TiO_2-urea in visible light (λ > 400 nm). N, F-TiO_2-urea shows a maximum hydrogen evolution of 400 μmol/g of the catalyst with a rate of ~60 μmol/g/h without the loading of any noble metal or other cocatalyst. To the best of our knowledge, this value of H_2 evolution is the highest reported so far under visible light illumination for TiO_2 without any cocatalyst. Under similar conditions, undoped TiO_2 and P-25 do not show any H_2 evolution. The inset of Figure 7 shows the H_2 evolution of N-doped TiO_2 and N, F-TiO_2-complex samples. N-doped TiO_2 shows H_2 evolution of 37 μmol/g, much lesser than that of N, F-TiO_2-urea. Defect sites are known to act as recombination centers for photogenerated electrons and holes.[42] As already discussed, PL emission of N-doped TiO_2 shows a broad band due to oxygen vacancy; thus, lesser yield of H_2 in N-TiO_2 can be attributed to the faster recombination of electron−hole at the defect sites. Li et al.[43] also found that photocatalytic activity of TiO_2 decreases with increase in defect-related PL emission. The N, F-TiO_2-complex shows a relatively higher value of H_2 evolution (180 μmol/g) compared to N-TiO_2 but yet smaller than N, F-TiO_2-urea, the latter having a higher N and F content and greater absorption in the visible region.

Results from Theory. We now turn to the results of our first-principles calculations. In these calculations, we considered three kinds of anionic substitutions in TiO_2: (a) nitrogen-substituted TiO_2 (N-TiO_2), (b) fluorine-substituted TiO_2 (F-TiO_2), and (c) nitrogen and fluorine-cosubstituted TiO_2 (N, F-TiO_2). To simulate the doping levels achieved in experiments, we used a 2 × 2 × 1 periodic supercell with 48 atoms ($Ti_{16}O_{32}$) with substitution of (a) 2 of the oxygen atoms with nitrogen atoms (6.25% N) for N-TiO_2, (b) 2 of the oxygen atoms by fluorine atoms (6.25% F) for F-TiO_2, and (c) 4 of the oxygen atoms with 2 nitrogen atoms and 2 fluorine atoms (6.25% F, 6.25% N) for N, F-TiO_2. Since the number of possible configurations of ordering of nitrogen and fluorine in these systems is large, we used one representative configuration in each case, except in the case of N, F-TiO_2 where we compared a few distinct configurations to determine the nature of ordering preferred by nitrogen and fluorine. In our calculations on water splitting on the (001) and (101) surfaces using SIESTA, we used a single-layer slab of N, F-TiO_2 with 2 × 2 surface cells and a vacuum of ~15 Å. A water molecule was placed parallel to the surface with its oxygen about 2.2 Å above a five-coordinated Ti site (referred to as "Ti(5c)") and the substituted nitrogen atom lying close to the surface. To sample

dx.doi.org/10.1021/ic401426q | Inorg. Chem. 2013, 52, 10512−10519

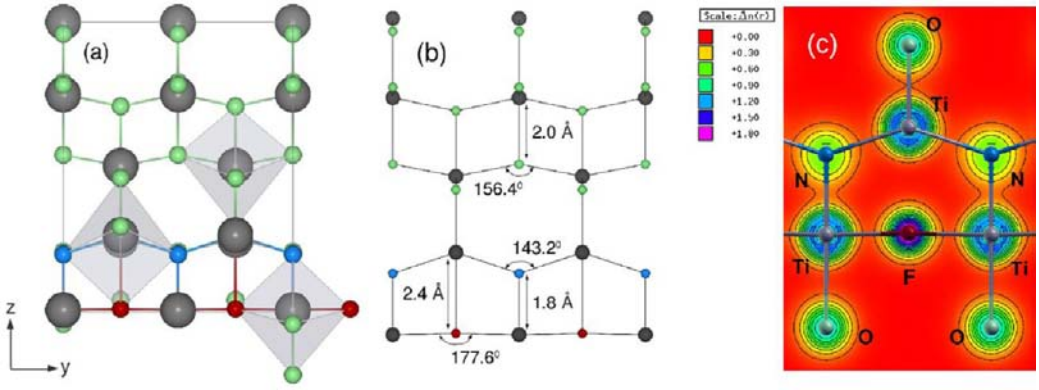

Figure 8. Structure of N, F-TiO_2 showing (a) Ti in three differently coordinated octahedral environments, (b) the local distortions caused by nitrogen and fluorine cosubstitution, and (c) contours of electronic charge density on the (100) plane (Ti = gray, O = green, N = blue, F = maroon).

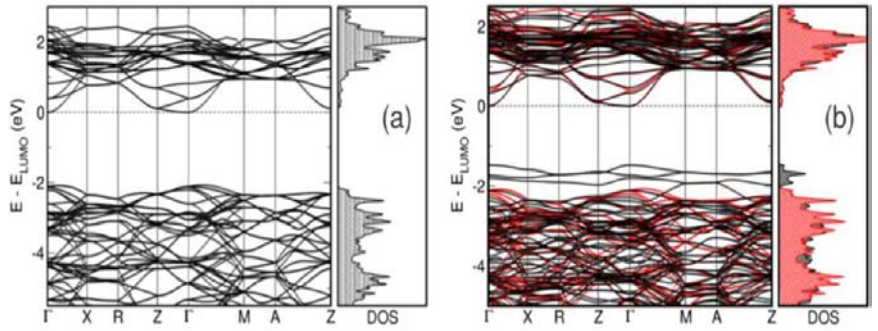

Figure 9. (a) Electronic band structure of bulk, undoped TiO_2 and (b) comparison of the band structures of pure TiO_2 (in red) and N, F-TiO_2 (in black). The N 2p-derived sub-band above the valence band is clearly visible.

integrations over the Brillouin zone of the supercell, we used a uniform k-mesh of 5 × 5 × 4 in ESPRESSO-based calculations, and 2 × 6 × 2 (for (101) surface) and 4 × 4 × 1 (for (001) surface) in SIESTA-based calculations. In all the cases, structural relaxation was carried out through energy minimization until the Hellman−Feynman forces on the atoms were within 0.05 eV/Å and the stresses were within 1 kbar.

Structure and Chemical Ordering. Our calculated lattice parameters of bulk anatase TiO_2 are a = 3.74 Å, c = 9.42 Å, u = 0.209, within the typical LDA errors and in good agreement with the experimental and published theoretical values.[44,45] The change in lattice parameters upon substitution with nitrogen and fluorine at oxygen sites is small (within 0.9% of those calculated for bulk TiO_2). On the other hand, there are significant local structural distortions in N, F-TiO_2 induced at the sites of substitutions (Figure 8a). The Ti−N bond length along the c-axis is 1.82 Å, while the length of the Ti−F bond is 2.40 Å. Notably, these are 7.5% shorter and 22.3% longer, respectively, relative to the Ti−O bonds (1.96 Å) in bulk TiO_2. The changes in the bond lengths of Ti−N and Ti−F bonds along the *ab*-plane are somewhat less dramatic and are about 3.7% and −1.5%, respectively, leading to smaller Ti−N−Ti (143.2°) and larger Ti−F−Ti (177.6°) bond angles, in comparison with Ti−O−Ti bond angles in bulk TiO_2 (156.4°) (Figure 8b). These structural changes suggest that the behavior of nitrogen and fluorine is like negative and positive charges respectively in N, F-TiO_2. These local distortions are more pronounced in N, F-TiO_2 than in F-TiO_2 and N-TiO_2, indicating that nitrogen and fluorine cosubstitution reinforces the effects of their substitution individually and gives greater stability.

The energetics of N-TiO_2, F-TiO_2, and N, F-TiO_2 reveal that (a) cosubstitution with nitrogen and fluorine is preferred over individual dopant substitutions with a lowering of energy by 1.93 eV per (N, F) pair. (b) Further substitution with excess nitrogen in N, F-TiO_2 is favored with a lowering of energy by 1.59 eV for an additional substituted nitrogen. The energies of different chemically ordered configurations of N, F-TiO_2 (with additional nitrogen substitution) suggest that (a) nitrogen and fluorine prefer nearest neighbor sites, being bonded to a cation (Ti) and (b) two nitrogen (or two fluorine) anions occupying such nearest neighbor sites are energetically unfavorable. This observation is not unexpected, as the nature of electrostatic interactions between nitrogen and fluorine would favor such pairwise clustering behavior.

The local structural changes at the substituted nitrogen and fluorine sites in TiO_2 are reflected in the electronic structure. The electronic charge density contours (Figure 8c) clearly reveal (a) a greater covalency in the Ti−N bond and that the chemical environment around nitrogen is anisotropic; (b) the spherical symmetry of the charge around fluorine, which reflects that the electronic orbitals of fluorine are completely filled, and the associated bonding is mostly ionic in nature; (c) weakening (lengthening) of bonding between oxygen and the Ti bonded to N with a relatively strong and covalent Ti−N bond.

Our calculated band structure of bulk TiO_2 (Figure 9a) is in good agreement with published LDA calculations,[45] with an indirect band gap of 2.06 eV at 0.29 Σ (in the Γ to X direction) comparable to earlier theoretical estimates.[46] Underestimation of the band gap with respect to the reported experimental value of 3.23 eV is typical of the calculation based on DFT-LDA

dx.doi.org/10.1021/ic401426q | *Inorg. Chem.* 2013, 52, 10512−10519

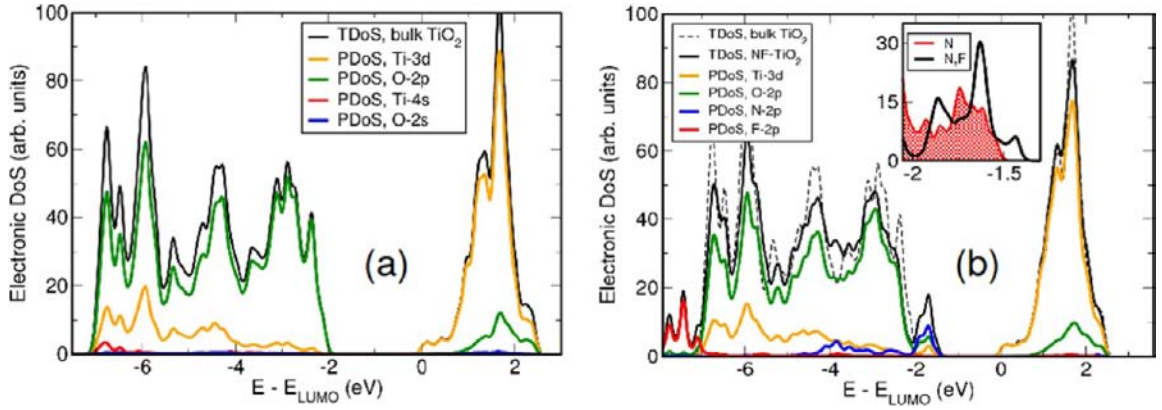

Figure 10. Density of electronic states projected onto atomic orbitals in (a) bulk, undoped TiO_2 and (b) N, F-co-substituted TiO_2. The inset in (b) is a comparison between the total density of electronic states (at the top of the valence band) of N-TiO_2 and N, F-TiO_2, clearly showing the enhancement in the sub-band due to fluorine cosubstitution.

functional. The band structure of a representative N, F-TiO_2 (Figure 9b) shows an isolated occupied band split weakly from the rest of the valence bands, leading to a *direct* and considerably reduced gap of 1.48 eV at Γ. From the hybrid exchange functional calculations on a 2 × 2 × 1 mesh of Bloch vectors, we estimate the correction to the band gaps and add it to our LDA estimates obtained using a much finer mesh of k-vectors. Thus, the corrected band gaps of pure TiO_2 (3.92 eV) and N, F-TiO_2 (3.06 eV) are slightly overestimated in comparison with the experimentally measured values (3.20 and 2.28 eV, respectively), but they succeed in capturing more accurately the change in the band gap upon nitrogen and fluorine cosubstitution. This reduction in the electronic band gap is essential and partially responsible for the improved photocatalytic activity of TiO_2 after cosubstitution with nitrogen and fluorine.

To understand the nature of this isolated sub-band at the top of the valence band, we analyzed the density of electronic states of bulk TiO_2 and N, F-TiO_2, by projecting it onto atomic orbitals. In bulk TiO_2, the valence band is constituted primarily of O 2p orbitals with a little mixing with the Ti 3d states while the lowest energy conduction bands are predominantly Ti 3d in character (Figure 10a). The uppermost valence bands are most affected by N, F substitution, with the N 2p-derived states arising as a sub-band with a bandwidth of about 0.6 eV, at the top of the valence band (with weaker contributions from the Ti 3d- and the O 2p-derived states), thereby effectively reducing the band gap (Figure 10b). Our analysis of the density of electronic states of N-TiO_2, F-TiO_2, and N, F-TiO_2 reveals that (a) p states of the strongly electronegative fluorine atoms are deep-lying in energy (∼6 eV lower than the valence band maximum; Figure 10b) while those of the less electronegative nitrogen are concentrated at the top of the valence band. (b) Formation of the sub-band of p states of the nitrogen atoms (in N, F-TiO_2) at the top of the valence band is greatly enhanced by the fluorine cosubstitution (see the inset in Figure 10b). The lowest energy conduction bands are essentially unaffected by N, F cosubstitution and retain their Ti 3d character. From the visualization of the upper most valence states at the Γ-point, we confirm that the charge is localized largely on the nitrogen atoms and spread weakly onto the p orbitals of the nearest neighbor oxygen atoms (Figure 11). The nature of this wave function reveals a weak covalent π-interaction between p_x orbital of oxygen and d_{xz} orbital of Ti.

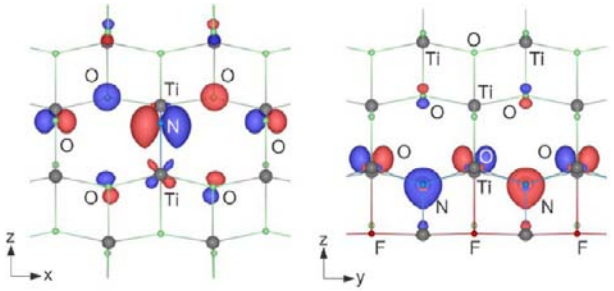

Figure 11. Visualization of the uppermost valence states of N, F-TiO_2 from *y*-direction (left) and *x*-direction (right) (Ti = gray, O = green, N = blue, F = maroon).

Born Effective Charges. The Born effective charge (BEC) tensor $Z^*_{i,\alpha\beta}$ of an atom in an insulator is defined as the atomic displacement $(u_{i,\beta})$ derivative of P[47]

$$Z^*_{i,\alpha\beta} = \frac{\partial P_\alpha}{\partial u_{i,\beta}} \quad (1)$$

where i runs over the atoms and α, β are Cartesian indices. The anomalous BECs of Ti in bulk TiO_2 ($Z^*_{xx} = Z^*_{yy} = 6.5$, $Z^*_{zz} = 5.7$) when compared to its nominal ionic charge of +4 is indicative of the hybridization of its d states with the p states of the surrounding oxygen ions and reflects a mixed covalent-ionic picture of bonding.[48] The anomalous BECs of oxygen ($Z^*_{xx} = -1.2$, $Z^*_{yy} = -5.4$, $Z^*_{zz} = -2.9$) in comparison with its nominal charge of −2 reveals a deviation from the purely ionic nature and a high anisotropy associated with the site, confirming our earlier conclusions based on our analysis of electronic density. In N, F-TiO_2, the BECs of nitrogen are $Z^*_{xx} = -1.2$, $Z^*_{yy} = -5.8$, $Z^*_{zz} = -3.9$, while those of fluorine are $Z^*_{xx} = -0.7$, $Z^*_{yy} = -3.2$, $Z^*_{zz} = -1.1$. This is consistent with the Ti−N−Ti and Ti−F−Ti chains seen along the *y*-direction and the π-like bonding interaction between the Ti 3d states and the N 2p states in the *z*-direction. The anomaly in the BEC tensor of Ti is stronger when it is bonded to nitrogen and weaker when bonded to fluorine. This clearly shows a relatively high chemical activity of N and relative inertness of F and confirms the mixed ionic−covalent and ionic nature of the Ti−N and Ti−F bonds respectively. Our calculations show an increase in the *z*-component of the electronic dielectric constant (the square of the refractive index) from 6.2 to 6.5, as another effect of the reduction in the electronic band gap on properties.

dx.doi.org/10.1021/ic401426q | *Inorg. Chem.* 2013, 52, 10512−10519

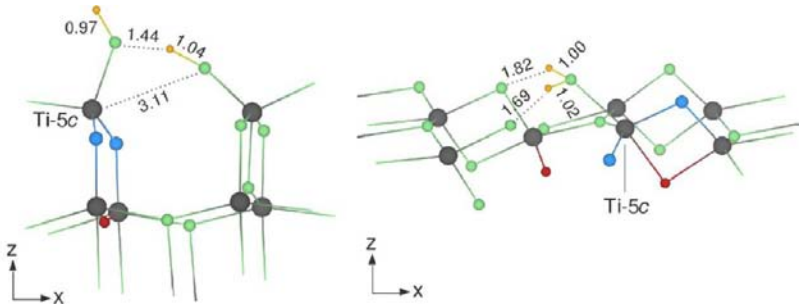

Figure 12. Interaction of a water molecule with the (a) (001) surface and (b) (101) surface of N, F-TiO_2. (All bond lengths shown are in angstrom. Ti = gray, O = green, N = blue, F = maroon, H = orange.)

Water Adsorption on the (001) and (101) Surfaces. In the case of pure anatase TiO_2, molecular adsorption of water occurs on the (101) surface while dissociative adsorption is favored on the (001) surface.[49] We have studied here the effect of nitrogen and fluorine cosubstitution on the nature of interaction of water with (001) and (101) surfaces of TiO_2. In both cases, we find that the strength of water molecules to adsorb on these surfaces increases significantly upon cosubstitution with nitrogen and fluorine, reflected in the increase in adsorption energies: from ~1.6 eV[49] to ~3.6 eV for the (001) surface, and from ~0.7 eV[49] to ~2.0 eV for the (101) surface. Moreover, in the case of the (001) surface of N, F-TiO_2, we find that there is formation of an intermediate complex, characterized by a weakened bond (3.11 Å) between an oxygen (fluorine) atom and the Ti(5c) atom involved in the adsorptive interaction. As a result, this activated oxygen (fluorine) forms a bond (1.04 Å) with a hydrogen atom of the water molecule (Figure 12a). The O−H bond lengths of the strained water molecule are 0.97 and 1.44 Å, the latter hydrogen being bonded to the activated oxygen (fluorine) atom. This is the intermediate state preempting the dissociation of the water molecule.

In the case of the (101) surface too, we observe structural changes contributing toward enhanced catalytic activity: a water molecule relaxes to a position favoring bonding interaction between its hydrogen atoms and two neighboring oxygen (fluorine) atoms on the surface (with O−H bond lengths of 1.69 and 1.82 Å, see Figure 12b). The corresponding O−H bond lengths of the strained water molecule are 1.02 and 1.00 Å (in contrast with 0.97 Å for an isolated molecule), making it relatively easier to photolyze. The chemical origin of these structural changes lies in the relatively stronger bond between the Ti(5c) atom and a nitrogen atom substituted at the neighboring site, leading to weakening of the Ti(5c)−O(F) bond (see our analysis based on charge density). The latter is broken with ease, and the oxygen (fluorine) atom bonds with a hydrogen atom of the water molecule. Thus, a weaker Ti(5c)−O(F) bond and the associated structural changes contribute toward relatively enhanced water dissociation capabilities of N, F-TiO_2. Second, the sub-band due to N 2p-derived states at the top of the valence band, further pronounced by fluorine cosubstitution, facilitates absorption of a photon and subsequent electron transfer to a water molecule, thereby increasing the ease with which water is split into hydrogen and oxygen. These factors, combined with the reduced electronic band gap, result in the enhancement of the photocatalytic activity of TiO_2 upon cosubstitution with nitrogen and fluorine.

CONCLUSIONS

A simple route to synthesize the anatase phase of N, F-TiO_2 using urea and ammonium fluoride as nitrogen and fluorine sources respectively has been described. The composition of this phase is found to be $TiO_{1.7}N_{0.18}F_{0.12}$. A lower saturation magnetization of the N, F-TiO_2-urea sample compared to nitrogen-doped TiO_2 is attributed to the absence of oxygen vacancies as revealed from photoluminescence spectroscopy. A significant reduction in the band gap on cosubstitution with nitrogen and fluorine, accompanied by the yellow coloration, is observed. Significant hydrogen evolution (400 μmol/g) from water is observed with N, F-TiO_2-urea on visible light irradiation, due to the enhanced visible light absorption. Our first-principles calculations show that cosubstitution of oxygen with nitrogen and fluorine is preferred over their individual substitution in TiO_2, with nitrogen and fluorine preferably occupying nearest neighbor sites. The p orbitals of nitrogen are most effective in altering the electronic structure of TiO_2, giving rise to a sub-band at the top of the valence band, the effect being enhanced by the presence of fluorine. We observe significant local distortion in the N, F-doped TiO_2 crystal, reflected in the anomalous Born charges of different atomic sites. They indicate that nitrogen and fluorine tend to act like negative and positive charge centers, respectively, and reinforce the effects of their individual substitution. Though our LDA calculations underestimate the band gap and the associated changes, they provide a clear picture of the structural and electronic changes caused in TiO_2 due to the cosubstitution by nitrogen and fluorine. Our calculations on water adorption on the (001) and (101) surfaces on N, F-TiO_2 show that the strong Ti−N bond weakens the bond between that Ti and the neighboring anion, facilitating the formation of a hydrogen bond between that anion and a hydrogen of the adsorbed water molecule, easing the dissociation of water and thereby increasing the photocatalytic activity of N, F-TiO_2.

AUTHOR INFORMATION

Corresponding Author

*E-mail address: cnrrao@jncasr.ac.in.

Notes

The authors declare no competing financial interest.

ACKNOWLEDGMENTS

N.K. and A.S. acknowledge MICINN (Spanish Ministry of Science and Innovation)/DST (Indian Department of Science and Technology) joint project for funding.

REFERENCES

(1) Zhang, Z.; Luo, Z.; Yang, Z.; Zhang, S.; Zhang, Y.; Zhou, Y.; Wang, X.; Fu, X. *RSC Adv.* **2013**, *3*, 7215.
(2) Balcerski, W.; Ryu, S. Y.; Hoffmann, M. R. *J. Phys. Chem. C* **2007**, *111*, 15357.
(3) Sathish, M.; Viswanathan, B.; Viswanath, R. P.; Gopinath, C. S. *Chem. Mater.* **2005**, *17*, 6349.
(4) Irie, H.; Watanabe, Y.; Hashimoto, K. *J. Phys. Chem. B* **2003**, *107*, 5483.
(5) Pan, J. H.; Cai, Z.; Yu, Y.; Zhao, X. S. *J. Mater. Chem.* **2011**, *21*, 11430.
(6) Yu, J.; Xiang, Q.; Ran, J.; Mann, S. *CrystEngComm* **2010**, *12*, 872.
(7) Yu, J.; Wang, W.; Cheng, B.; Su, B.-L. *J. Phys. Chem. C* **2009**, *113*, 6743.
(8) Hoang, S.; Guo, S.; Mullins, C. B. *J. Phys. Chem. C* **2012**, *116*, 23283.
(9) Meng, Q.; Wang, T.; Liu, E.; Ma, X.; Ge, Q.; Gong, J. *Phys. Chem. Chem. Phys.* **2013**, in press.
(10) Li, D.; Haneda, H.; Hishita, S.; Ohashi, N. *Chem. Mater.* **2005**, *17*, 2588.
(11) Wang, Q.; Chen, C.; Ma, W.; Zhu, H.; Zhao, J. *Chem.—Eur. J.* **2009**, *15*, 4765.
(12) Chen, D.; Jiang, Z.; Geng, J.; Zhu, J.; Yang, D. *J. Nanopart. Res.* **2009**, *11*, 303.
(13) Seibel Ii, H. A.; Karen, P.; Wagner, T. R.; Woodward, P. M. *J. Mater. Chem.* **2009**, *19*, 471.
(14) Liu, G.; Yang, H. G.; Wang, X.; Cheng, L.; Pan, J.; Lu, G. Q.; Cheng, H.-M. *J. Am. Chem. Soc.* **2009**, *131*, 12868.
(15) Maeda, K.; Shimodaira, Y.; Lee, B.; Teramura, K.; Lu, D.; Kobayashi, H.; Domen, K. *J. Phys. Chem. C* **2007**, *111*, 18264.
(16) Niewa, R.; DiSalvo, F. J. *Chem. Mater.* **1998**, *10*, 2733.
(17) Fuertes, A. *Dalton Trans.* **2010**, *39*, 5942.
(18) Zhang, J.; Wu, Y.; Xing, M.; Leghari, S. A. K.; Sajjad, S. *Energy Environ. Sc.* **2010**, *3*, 715.
(19) Zhao, H.; Lei, M.; Chen, X.; Tang, W. *J. Mater. Chem.* **2006**, *16*, 4407.
(20) Gomathi, A.; Sundaresan, A.; Rao, C. N. R. *J. Solid State Chem.* **2007**, *180*, 291.
(21) Gomathi, A.; Reshma, S.; Rao, C. N. R. *J. Solid State Chem.* **2009**, *182*, 72.
(22) Giordano, C.; Erpen, C.; Yao, W.; Antonietti, M. *Nano Lett.* **2008**, *8*, 4659.
(23) Giordano, C.; Erpen, C.; Yao, W.; Milke, B.; Antonietti, M. *Chem. Mater.* **2009**, *21*, 5136.
(24) Han, S.; Choi, S.-H.; Kim, S.-S.; Cho, M.; Jang, B.; Kim, D.-Y.; Yoon, J.; Hyeon, T. *Small* **2005**, *1*, 812.
(25) Seibel, H. A.; Karen, P.; Wagner, T. R.; Woodward, P. M. *J. Mater. Chem.* **2009**, *19*, 471.
(26) Rodríguez-Carvajal, J. *Physica B* **1993**, *192*, 55.
(27) Giannozzi, P.; Baroni, S.; Bonini, N.; Calandra, M.; Car, R.; Cavazzoni, C.; Ceresoli, D.; Chiarotti, G. L.; Cococcioni, M.; Dabo, I.; Dal Corso, A.; de Gironcoli, S.; Fabris, S.; Fratesi, G.; Gebauer, R.; Gerstmann, U.; Gougoussis, C.; Kokalj, A.; Lazzeri, M.; Martin-Samos, L.; Marzari, N.; Mauri, F.; Mazzarello, R.; Paolini, S.; Pasquarello, A.; Paulatto, L.; Sbraccia, C.; Scandolo, S.; Sclauzero, G.; Seitsonen, A. P.; Smogunov, A.; Umari, P.; Wentzcovitch, R. M. *J. Phys.: Condens. Matter* **2009**, *21*, 395502.
(28) Soler, J. M.; Artacho, E.; Gale, J. D.; García, A.; Junquera, J.; Ordejón, P.; Sánchez-Portal, D. *J. Phys.: Condens. Matter* **2002**, *14*, 2745.
(29) Vanderbilt, D. *Phys. Rev. B* **1990**, *41*, 7892.
(30) Perdew, J. P.; Zunger, A. *Phys. Rev. B* **1981**, *23*, 5048.
(31) Heyd, J.; Scuseria, G. E.; Ernzerhof, M. *J. Chem. Phys.* **2003**, *118*, 8207.
(32) Troullier, N.; Martins, J. L. *Phys. Rev. B* **1991**, *43*, 1993.
(33) Ceperley, D. M.; Alder, B. J. *Phys. Rev. Lett.* **1980**, *45*, 566.
(34) Saha, N. C.; Tompkins, H. G. *J. Appl. Phys.* **1992**, *72*, 3072.
(35) Guosheng, W.; Jiali, W.; Samantha, N.; Aicheng, C. *Nanotechnology* **2010**, *21*, 085701.
(36) Wu, G.; Wen, J.; Nigro, S.; Chen, A. *Nanotechnology* **2010**, *21*, 085701.
(37) Li, X.; Gao, C.; Wang, J.; Lu, B.; Chen, W.; Song, J.; Zhang, S.; Zhang, Z.; Pan, X.; Xie, E. *J. Power Sources* **2012**, *214*, 244.
(38) Wu, Z.; Dong, F.; Zhao, W.; Guo, S. *J. Hazard. Mater.* **2008**, *157*, 57.
(39) Sundaresan, A.; Bhargavi, R.; Rangarajan, N.; Siddesh, U.; Rao, C. N. R. *Phys. Rev. B* **2006**, *74*, 161306.
(40) Sundaresan, A.; Rao, C. N. R. *Nano Today* **2009**, *4*, 96.
(41) Yu, L.; Xi, J.; Li, M.-D.; Chan, H. T.; Su, T.; Phillips, D. L.; Chan, W. K. *Phys. Chem. Chem. Phys.* **2012**, *14*, 3589.
(42) Kudo, A.; Miseki, Y. *Chem. Soc. Rev.* **2009**, *38*, 253.
(43) Li, X. Z.; Li, F. B.; Yang, C. L.; Ge, W. K. *J. Photochem. Photobiol., A* **2001**, *141*, 209.
(44) Rao, K. V. K.; Naidu, S. V. N.; Iyengar, L. *J. Am. Ceram. Soc.* **1970**, *53*, 124.
(45) Mikami, M.; Nakamura, S.; Kitao, O.; Arakawa, H.; Gonze, X. *Jpn. J. Appl. Phys.* **2000**, *39*, 847.
(46) Mo, S.-D.; Ching, W. Y. *Phys. Rev. B* **1995**, *51*, 13023.
(47) Gonze, X.; Lee, C. *Phys. Rev. B* **1997**, *55*, 10355.
(48) Ghosez, P.; Michenaud, J. P.; Gonze, X. *Phys. Rev. B* **1998**, *58*, 6224.
(49) Vittadini, A.; Selloni, A.; Rotzinger, F. P.; Grätzel, M. *Phys. Rev. Lett.* **1998**, *81*, 2954.